High-fidelity quantum gates in Si/SiGe double quantum dots

Maximilian Russ, D. M. Zajac, A. J. Sigillito, F. Borjans, J. M. Taylor, J. R. Petta, and Guido Burkard

Phys. Rev. B **97**, 085421 — Published 15 February 2018

DOI: 10.1103/PhysRevB.97.085421

High-fidelity quantum gates in Si/SiGe double quantum dots

Maximilian Russ,[1] D. M. Zajac,[2] A. J. Sigillito,[2] F. Borjans,[2] J. M. Taylor,[3] J. R. Petta,[2] and Guido Burkard[1]

[1] *Department of Physics, University of Konstanz, D-78457 Konstanz, Germany*
[2] *Department of Physics, Princeton University, Princeton, New Jersey 08544, USA*
[3] *Joint Quantum Institute and Joint Center for Quantum Information and Computer Science, NIST and University of Maryland, College Park, Maryland 20742, USA*

(Dated: January 23, 2018)

Motivated by recent experiments of Zajac *et al.*[1], we theoretically describe high-fidelity two-qubit gates using the exchange interaction between the spins in neighboring quantum dots subject to a magnetic field gradient. We use a combination of analytical calculations and numerical simulations to provide the optimal pulse sequences and parameter settings for the gate operation. We present a novel synchronization method which avoids detrimental spin flips during the gate operation and provide details about phase mismatches accumulated during the two-qubit gates which occur due to residual exchange interaction, non-adiabatic pulses, and off-resonant driving. By adjusting the gate times, synchronizing the resonant and off-resonant transitions, and compensating these phase mismatches by phase control, the overall gate fidelity can be increased significantly.

I. INTRODUCTION

Spin qubits[2] implemented in silicon quantum dots[3] are a viable candidate for enabling quantum error corrected quantum computation due to their long coherence times[4–7] and high-fidelity qubit manipulation[1,8,9]. Experiments using isotopically enriched silicon show single-qubit fidelities $F > 99.9\%$[10] thus exceeding the threshold of quantum-error correction[11]. Successful demonstrations of two-qubit gates[1,7,9,12], however, show fidelities far below the fault-tolerant threshold, therefore being the limiting factor for large-scale quantum computation. Here, based on the state-of-the-art quantum devices[13], we show a way to implement high-speed and high-fidelity two-qubit gates.

High-speed and high-fidelity single-qubit gate operations are achieved using electric dipole spin resonance (EDSR) by shifting the electron position in a slanting magnetic field through the modulation of the electrostatic gate voltages[1,9,10,12,14,15]. Interconnecting multiple spin qubits is possible through the exchange interaction between electrons in adjacent quantum dots[2,16,17]. However, the fidelity of these gates is strongly limited by charge noise, which is induced by electric fluctuations of the system, and gives rise to substantial gate operation errors[12,18]. Higher fidelities can be achieved if the system is operated at a symmetric operation point or sweet spot, where the exchange coupling is first-order insensitive to electric fluctuations[19–23]. Alternatively, combining exchange with a strong magnetic field gradient between the electron spins in the dot[1,9] suppresses the dominating dephasing processes through the large energy splitting of the two-qubit states[24]. Two explicit implementations for two-qubit gates have been successfully demonstrated, an ac pulsed frequency-selective CNOT gate[1,9] and a dc pulsed CZ gate[9,25,26]. These realizations are still not perfect, both acquiring local phases on the individual spin during the gate-operation due to unitary and non-unitary effects, e.g. charge noise, which have to be identified and compensated. The reduction of the overall gate fidelity due to off-resonant driving still remains an issue without the use of complex pulse shaping[27,28].

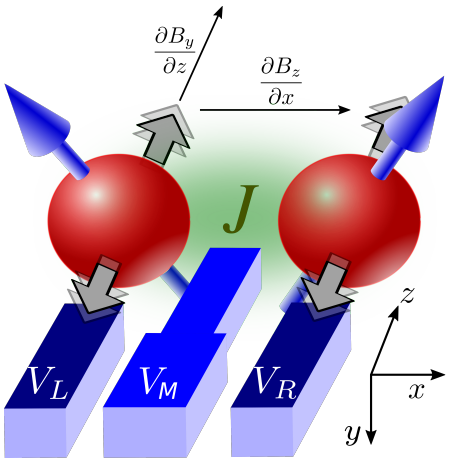

FIG. 1. Illustration of a gate defined double quantum dot (DQD) occupied with two electron spins inside a large homogenous magnetic field (not shown) and an anisotropic magnetic field $\boldsymbol{B}$ from a micromagnet. A gradient $\frac{\partial B_z}{\partial x}$ along the double dot axis (x-direction) gives rise to distinguishable spin resonance frequencies. Periodic modulation of the gate voltages (V_L and V_R) shifts the electron position in the z-direction (in plane) which generates an oscillating magnetic field in the motion-frame of the electrons due to the gradient $\frac{\partial B_y}{\partial z}$. An electrostatic barrier gate V_M allows for precise control over the exchange interaction J between the spins.

In this paper, we address both the dc CZ gate and the ac CNOT gate, and propose several step towards implementing high-fidelity gates. These steps include adding an echo pulse, synchronizing the resonant and off-resonant Rabi frequencies, and identifying local phases that the individual spins acquire during the gate operation. The paper is structured as follows. In section II, we begin with the theoretical description of our system. Subsequently, we model the dc pulsed CZ gate (section III)

and present a high-fidelity implementation in subsection III A. Then, we describe the ac pulsed frequency-selective CNOT gate (section IV), provide a synchronized high-fidelity implementation in subsection IV A, and show its performance under the influence of charge noise in subsection IV B. In section V, we conclude our paper with a summary and an outlook.

II. THEORETICAL MODEL

Our theoretical investigation is inspired by the experiments of Ref.[1], therefore, we use the same terminology for the theoretical description. The setup (see Fig. 1) consists of two gate defined quantum dots in a Si/SiGe heterostructure operated in the (1,1) regime where (n_L, n_R) is defined as the charge configuration with n_L electrons in the left and n_R electrons in the right dot. The methods presented in the following can be applied to quantum dots in other materials as well. A middle barrier gate is biased with voltage V_M to tune the exchange interaction J between the two spins. For our theoretical description we use the Heisenberg Hamiltonian of two neighboring spins that are placed in an inhomogeneous magnetic field

$$H(t) = J(t)(\boldsymbol{S}_L \cdot \boldsymbol{S}_R - 1/4) + \boldsymbol{S}_L \cdot \boldsymbol{B}_L + \boldsymbol{S}_R \cdot \boldsymbol{B}_R. \quad (1)$$

Here $J(t)$ describes the time-dependent Heisenberg exchange interaction between the spin of the electron on the left dot, $\boldsymbol{S}_L$, and the spin of the electron on the right dot, $\boldsymbol{S}_R$, resulting from the hybridization of the singlet electron wave-function with the additional charge states, (2,0) and (0,2). In the Hubbard limit, in the (1,1) charge configuration, exchange is given by $J = 2t_M^2(U_L + U_R)/[(U_L + \varepsilon)(U_R - \varepsilon)]$ where $t_M = t_M(V_M)$ is the tunneling matrix element between the electron spins which depends on the middle barrier voltage V_M, $\varepsilon \propto (V_L - V_R)/2$ is the single-particle detuning between the energy levels of the two spins set by V_L and V_R, and U_L and U_R are the respective charging energies in the dots. Here, $\varepsilon = 0$ corresponds to the center of the (1,1) charge regime. Either biasing the DQD, thus, changing ε, or barrier control, changing V_M, yields control over the exchange interaction with barrier control being superior if operated at a charge noise sweet spot[20,21,29] near the center of the (1,1) charge region.

The remaining terms in the Hamiltonian (1) describe the interaction between the spin and the magnetic field (in energy units) $\boldsymbol{B}_L = (0, B_y^L(t), B_z^h + B_z^L)^T$ and $\boldsymbol{B}_R = (0, B_y^R(t), B_z^h + B_z^R)^T$. The field consists of the homogeneous component B_z^h which lifts the spin degeneracy, and an inhomogeneous field produced by the micromagnet B_z^Q $(Q = L, R)$ that leads to distinct ESR frequencies for the left and right spin allowing one to individually address each spin. A transverse time-dependent field

$$B_y^Q(t) = B_y^{Q,0} + B_y^{Q,1}\cos(\omega t + \theta) \quad (2)$$

occurs from the shift of the electron position in the slanting magnetic field along x-direction. This last contribution is further composed of a small static part, $B_y^{Q,0}$ and a dynamic coupling term, $B_y^{Q,1}$ due to an electrostatic modulation of the electrostatic gates, V_L and V_R, with frequency ω. The contribution of the static part, $B_y^{Q,0} \ll |\boldsymbol{B}_L - \boldsymbol{B}_R|$, will drop out in the rotating wave approximation with frequency ω, and is therefore neglected in the following.

Addressing each spin as a separate qubit, the Hamiltonian (1) can be written in the two-qubit basis $\{|\uparrow\uparrow\rangle, |\uparrow\downarrow\rangle, |\downarrow\uparrow\rangle, |\downarrow\downarrow\rangle\}$ as follows;

$$H(t) = \begin{pmatrix} E_z & -\mathrm{i}B_y^R(t) & -\mathrm{i}B_y^L(t) & 0 \\ \mathrm{i}B_y^R(t) & -(\delta E_z + J)/2 & J/2 & -\mathrm{i}B_y^L(t) \\ \mathrm{i}B_y^L(t) & J/2 & (\delta E_z - J)/2 & -\mathrm{i}B_y^R(t) \\ 0 & \mathrm{i}B_y^L(t) & \mathrm{i}B_y^R(t) & -E_z \end{pmatrix}. \quad (3)$$

Here we introduced the difference and the average Zeeman splitting $\delta E_z = B_z^R - B_z^L$ and $E_z = B_z^h + (B_z^L + B_z^R)/2$. In the absence of exchange, $J \approx 0$, single qubit operations are possible by matching ω with the resonance frequency, $B_z^h + B_z^L$ $(B_z^h + B_z^R)$, of the left (right) dot. This corresponds to regime II in Fig. 2. A large δE_z is beneficial since it widely separates both resonances in energy allowing for stronger driving, thus, faster gate operations.

III. DC ENTANGLING GATES: PULSED EXCHANGE

Two-qubit gates between neighboring single-spin qubits are realizable using the exchange interaction between the spins[2,18] with or without a magnetic field gradient[25,26]. If the exchange energy dominates the Hamiltonian (3), i.e. $J \gg \delta E_z$, the (approximate) two-qubit eigenstates are the spin singlet, $|\uparrow\downarrow\rangle - |\downarrow\uparrow\rangle$ and triplets, $|\uparrow\uparrow\rangle$, $|\uparrow\downarrow\rangle + |\downarrow\uparrow\rangle$, $|\downarrow\downarrow\rangle$, and the resulting operation yields (for $\delta E_z = 0$) the entangling $\sqrt{\mathrm{SWAP}}$-gate. Sequential implementation of two $\sqrt{\mathrm{SWAP}}$-gates and single-qubit rotations yields a CNOT-gate[2]. In the case of weak exchange, i.e. $J \ll \delta E_z$, the two-qubit states are effectively the product states $|\uparrow\uparrow\rangle$, $|\widetilde{\uparrow\downarrow}\rangle$, $|\widetilde{\downarrow\uparrow}\rangle$, $|\downarrow\downarrow\rangle$ with small corrections in $|\widetilde{\uparrow\downarrow}\rangle$ and $|\widetilde{\downarrow\uparrow}\rangle$ due to the exchange interaction. In this limit the exchange interaction yields a conditional phase (CPHASE) gate. In this paper we focus on the regime $J \ll \delta E_z$ which is typical for DQD systems in the presence of a micromagnet. However, for adiabatic pulses, with ramp time $\tau_r \gg J/\delta E_z^2$, both implementations are equivalent. The definition of the ramp time τ_r is illustrated in Fig. 2 (b) and (c). Note that the criteria for the adiabatic regime is usually fulfilled in state-of-the-art devices[1,9,10]. For an adiabatic pulse the instantaneous

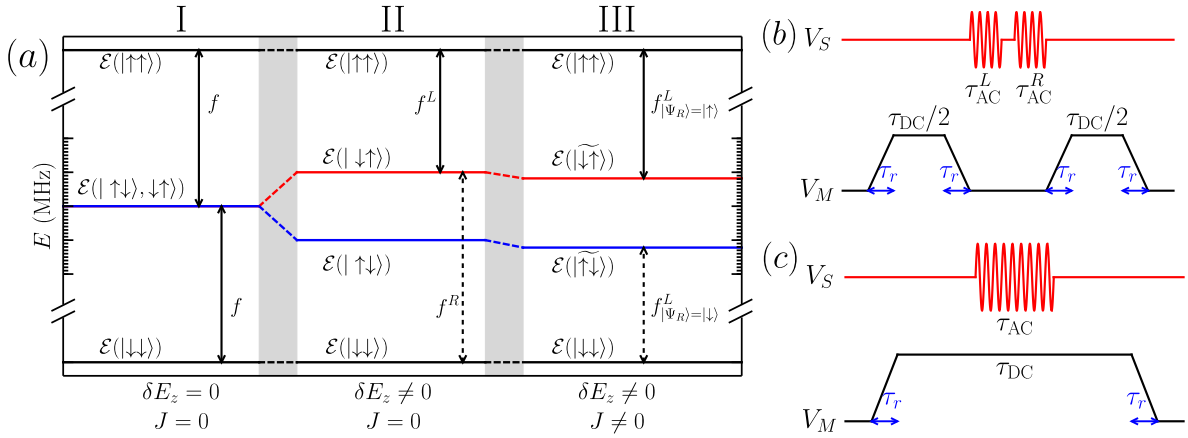

FIG. 2. (a) Eigenenergies $\mathcal{E}$ of two spins in a double quantum dot in the presence of a magnetic field gradient and relevant transitions between them for three distinct[1] parameter regimes. Regime I describes the case without a magnetic field gradient in which all single-spin flip transitions are energetically degenerate. In the presence of a field gradient (Regime II) the degeneracy of the transition frequencies between the left (solid-line arrow) and right spin (dashed-line arrow) is lifted, making it possible to energetically distinguish between single-qubit operations on the left and right spin. Turning on the exchange interaction, $J \ll \delta E_z$, (Regime III) further distinguishes conditional spin-flips from each other, i.e. the left ESR resonance frequency now depends on the right spin state, thus, allowing for frequency-selective entangling two-qubit gates. Such conditional spin flip operations are possible, e.g., by resonantly driving the transition $|\uparrow\uparrow\rangle \leftrightarrow |\widetilde{\downarrow\uparrow}\rangle$ to perform a single-shot CNOT gate. Since the eigenstates $\mathcal{E}(|\widetilde{\downarrow\uparrow}\rangle)$ and $\mathcal{E}(|\widetilde{\uparrow\downarrow}\rangle)$ are both energetically lowered (by $J/2$ for $J \ll \delta E_z$) the transition $|\downarrow\downarrow\rangle \leftrightarrow |\widetilde{\uparrow\downarrow}\rangle$ is detuned from resonance by $\sim J$. (b) Schematic pulse sequence of the spin-echo CZ gate described in subsection III A. Two adiabatic middle barrier pulses of length $\tau_{\rm DC}/2$ and ramp time τ_r are combined with two ac pulses of length $\tau^{L,R}_{\rm AC}$, performing a spin-flip on the left and right spin. (c) Schematic pulse sequence of the frequency selective CNOT gate. An adiabatic middle barrier pulse with length $\tau_{\rm DC}$ and ramp time τ_r is combined with an ac pulse of length $\tau_{\rm AC}$ resulting in a conditional spin-flip.

eigenvalues of the Hamiltonian (3) are given as follows:

$$\mathcal{E}(|\uparrow\uparrow\rangle) = E_z, \tag{4}$$

$$\mathcal{E}(|\widetilde{\uparrow\downarrow}\rangle) = \left(-J - \sqrt{J^2+\delta E_z^2}\right)/2, \tag{5}$$

$$\mathcal{E}(|\widetilde{\downarrow\uparrow}\rangle) = \left(-J + \sqrt{J^2+\delta E_z^2}\right)/2, \tag{6}$$

$$\mathcal{E}(|\downarrow\downarrow\rangle) = -E_z. \tag{7}$$

Figure 2 (a) shows the eigenenergies for three different parameter regimes. Note, that for $J \ll \delta E_z$ one can use the expansion $\sqrt{J^2+\delta E_z^2} \approx \delta E_z + \frac{J^2}{2\delta E_z}$ simplifying the expressions in Eqs. (5) and (6). The time evolution of an adiabatic exchange pulse of length τ in the rotating frame $\tilde{H}(t) = \tilde{R}^\dagger H \tilde{R} + \mathrm{i}\dot{\tilde{R}}^\dagger \tilde{R}$ with $\tilde{R} = \exp\left[-\mathrm{i}\omega t(S_{z,L}+S_{z,R})/\hbar\right]$ and $\hbar\omega = E_z/2$ is given by

$$U(\tau) = \mathrm{diag}\left[1,\ \mathrm{e}^{\mathrm{i}\left(\bar{J}+\bar{K}\right)\frac{\tau}{2\hbar}},\ \mathrm{e}^{\mathrm{i}\left(\bar{J}-\bar{K}\right)\frac{\tau}{2\hbar}}, 1\right]. \tag{8}$$

Here we define the average exchange $\bar{J} = \frac{1}{\tau}\int_0^\tau J(t)dt$ and an average effective gradient $\bar{K} = \frac{1}{\tau}\int_0^\tau \sqrt{J(t)^2+\delta E_z^2}dt$. The time evolution, up to a global phase, can be decomposed into two parts as $U = U_{\rm ent}U_{\rm loc}$ with an entangling term

$$U_{\rm ent}(\tau) = \exp\left(\mathrm{i}\bar{J}\tau\, S_{z,L}S_{z,R}/\hbar\right), \tag{9}$$

and an accumulated local phase

$$\begin{aligned} U_{\rm loc}(\tau) &= \exp\left(-\mathrm{i}\bar{K}(S_{z,L}-S_{z,R})\tau/\hbar\right) \\ &\approx \exp\left[-\mathrm{i}\left(\delta E_z + \frac{\bar{J}^2}{2\delta E_z}\right)(S_{z,L}-S_{z,R})\tau/\hbar\right]. \end{aligned} \tag{10}$$

For gate times being odd integer multiples of $\hbar\pi/\bar{J}$, $\tau = (2n+1)\hbar\pi/\bar{J}$ the time-evolution (9) is equivalent to CZ up to single-qubit z-rotations[26]. Even multiples, $\tau = \tau_{\rm DC} \equiv 2\hbar\pi n/\bar{J}$, correspondingly yield identity up to local S_z-rotations $\mathrm{e}^{\mathrm{i}\Phi_L S_{z,L}/2}$ and $\mathrm{e}^{\mathrm{i}\Phi_R S_{z,R}/2}$ for the left and right spin. From Eq. (10) we find the following expressions for the phases,

$$\Phi_L^{\rm DC} = -2\pi n\bar{K}/\bar{J}, \tag{11}$$

$$\Phi_R^{\rm DC} = 2\pi n\bar{K}/\bar{J}. \tag{12}$$

The correction of these phases will be discussed in subsection IV A. The fact that the dc CZ operation can be cancelled out will be important for the ac gate discussed in section IV.

A. High fidelity dc implementation

So far we have shown that we can implement two-qubit gates between both spins using the exchange interaction,

however there are several obstacles that need to be considered for a high-fidelity performance. We consider the inclusion of an echo mechanism for removing the excess phases in the exchange gate as well as potentially unknown magnetic gradients[30,31]. In the following we distinguish between adiabatic and non-adiabatic exchange pulses which both are experimentally feasible.

In the absence of exchange, $J \approx 0$, and electric driving, $B_y^Q(t) = 0$, the Hamiltonian (3) can be written in the following compact way

$$H_0 = E_z(S_{z,L} + S_{z,R}) + \delta E_z(S_{z,L} - S_{z,R})/2, \qquad (13)$$

which consists of two parts that both act in different subspaces. The E_z term only acts in the even parity space spanned by $\{|\uparrow,\uparrow\rangle, |\downarrow,\downarrow\rangle\}$ giving rise to fast oscillations, while the δE_z term only acts in the odd parity space spanned by $\{|\uparrow,\downarrow\rangle, |\downarrow,\uparrow\rangle\}$. For an efficient examination of the exchange dynamics, we define new Pauli operators, $\sigma_x = S_{+,L}S_{-,R} + H.c.$, $\sigma_z = S_{z,L} - S_{z,R}$, and the projector $P = (1 - 4S_{z,L}S_{z,R})/2$, acting only in the odd parity space. In a similar manner, we define the new Pauli operators, $\tau_z = S_{z,L} + S_{z,R}$ and $\tau_x = S_{+,L}S_{+,R} + S_{-,L}S_{-,R}$, acting only on the even parity subspace.

In this new basis, the (time-dependent) Hamiltonian (1) neglecting transverse gradient fields is

$$H(t) = E_z\tau_z + \delta E_z\sigma_z/2 - J(t)[P - \sigma_x]/2, \qquad (14)$$

with $J(t)$ being the externally controlled exchange. We also note that a π rotation of both spins about the x-axis corresponds, up to a global phase, to the unitary $\tau_x + \sigma_x$ while a pair of y-axis pulses would correspond to $\tau_x - \sigma_x$.

For both fast and slow exchange pulses of length T, we see that the even parity space only undergoes evolution according to $E_z\tau_z$, and thus will effectively factor out after inclusion of the π pulses shown in Fig. 2 (b). Meanwhile, the odd parity space undergoes nontrivial evolution, due to both the overall phase evolution $-\bar{J}T/2$ and from the rotation in the subspace about the axis $(J, 0, \delta E_z)$.

We first consider fast instantaneous exchange pulses, $\tau_r \ll J/\delta E_z^2$. The time evolution in the odd parity (P) subspace is then given by rotations for a controlled period about various axes. A simple exchange pulse corresponds to

$$U_J = (\mathbb{1} - P)e^{-iTE_z\tau_z/\hbar} + Pe^{i\Phi_x}\left[\cos(\Omega_J T) - i\frac{J\sigma_x + \delta E_z\sigma_z}{2\hbar\Omega_J}\sin(\Omega_J T)\right], \qquad (15)$$

with $\Omega_J = \sqrt{\delta E_z^2 + J^2}/(2\hbar)$. We note that for $\Omega_J T = n\pi$ with integer n, we obtain a CPHASE gate with phase $\Phi_x = \bar{J}Tn\pi/(2\Omega_J\hbar) = \frac{\bar{J}}{\sqrt{\delta E_z^2 + J^2}}n\pi$, as the sin term vanishes. This presents one way to remove the excess phase.

We now consider the full echo-sequence consisting of two exchange pulses and the rotations of individual spins in the middle of the sequence. Towards the end of this section, we would like to understand how this gate behaves in the rotating frame in which we apply our single qubit gates (motivated by experiment[1]). If we envision starting U_J at time t_1 and ending it at time $t_2 = t_1 + T$, we need to know the rotating frame state at the end of the sequence. We can move U_J to the rotating frame defined by $R(t) = e^{-i(\omega_1 S_{z,L} + \omega_2 S_{z,R})t}$ with the qubit frequencies $\omega_1 = (E_z + \delta E_z/2)/\hbar$ and $\omega_2 = (E_z - \delta E_z/2)/\hbar$ by applying the unitary transformation $|\psi_{\rm rf}(t)\rangle = R^\dagger(t)|\psi_{\rm lab}(t)\rangle$. Thus, we have

$$|\psi_{\rm rf}(t_2)\rangle = R^\dagger(t_2)U_J R(t_1)|\psi_{\rm rf}(t_1)\rangle = U_J^{\rm rf}(t_2, t_1)|\psi_{\rm rf}(t_1)\rangle, \qquad (16)$$

where we move back to the lab frame, apply U_J, then move back to the rotating frame.

In total, in the rotating frame, we find

$$U_J^{\rm rf}(t_1 + T, t_1) = (\mathbb{1} - P) + Pe^{i\Phi_x}e^{i\delta E_z T\sigma_z/4}\left[\cos(\Omega_J T) - i\frac{J\sigma_\mu + \delta E_z\sigma_z}{2\Omega_J}\sin(\Omega_J T)\right]e^{i\delta E_z T\sigma_z/4}, \qquad (17)$$

where $\sigma_\mu = \cos(\delta E_z(2t_1 + T)/2)\sigma_x + \sin(\delta E_z(2t_1 + T)/2)\sigma_y$. Thus the start time t_1 enters in the definition of the rotation axis $\boldsymbol{\mu} = (\cos(\delta E_z(2t_1+T)/2), \sin(\delta E_z(2t_1 + T)/2), 0)^T$. While we do not necessarily want any such rotation, as the diagonal term $\sim J$ will perform a CPHASE-like evolution, we will have to be careful to avoid unwanted effects from this evolution.

One approach for removing the spin-flip effect (σ_μ term in Eq. (17)) consists in switching $J(t)$ adiabatically, thus $\tau_r \gg J/\delta E_z^2$. Considering parameters from Ref.[1], the adiabatic condition corresponds to a rise time on the timescale of > 4 ns. Diagonalization of $H(t)$ in the rotating frame yields $\tilde{H}^{\rm rf} = -PJ(t)/2 + (\Omega_J(t) - \delta E_z/2)\sigma_z$ with $\Omega_J(t) = \sqrt{\delta E_z^2 + J(t)^2}/2$. Small non-adiabatic corrections enter with a σ_+ term, which behaves in a similar manner to the σ_x term given by U_J for the fast case. The net result of the adiabatic case in the rotating frame is

$$U_{\rm ad}^{\rm rf} = (1 - P) + Pe^{i\Phi_{\rm ad}}e^{-i\phi_z\sigma_z}, \qquad (18)$$

with $\Phi_{\rm ad} = \bar{J}T/2$ and $\phi_z = (\bar{K} - \delta E_z)T/2 = \int_0^T \sqrt{\delta E_z^2 + J(t)^2}dt/2 - \delta E_z T/2$. Thus we see that the adiabatic J pulse leads to an extra single qubit z rotation

for both spins, in addition to the desired CPHASE-like operation. Note, that this phase in the rotating frame of the individual spins is equivalent to the phase given by Eqs. (11) and (12) for $n = 1$.

We now consider a more general solution to the extra phase evolution (corresponding to a potentially undesired set of single qubit z rotations) as well as the extra rotation about the μ-axis. Specifically, we consider two π pulses about the x-axis on the qubits in between two CPHASE-like unitaries [see Fig. 2 (b)]. For the adiabatic case, we have

$$\begin{aligned} U_{c,\mathrm{ad}} &= U_{\mathrm{ad}}^{\mathrm{rf}}(4S_{x,L}S_{x,R})U_{\mathrm{ad}}^{\mathrm{rf}} && (19)\\ &= (4S_{x,L}S_{x,R})\left[(1-P)+P\mathrm{e}^{\mathrm{i}\Phi_{\mathrm{ad}}}\mathrm{e}^{\mathrm{i}\sigma_z\phi_z}\right] \\ &\quad\times\left[(1-P)+P\mathrm{e}^{\mathrm{i}\Phi_{\mathrm{ad}}}\mathrm{e}^{-\mathrm{i}\sigma_z\phi_z}\right] && (20)\\ &= (4S_{x,L}S_{x,R})\left[(1-P)+P\mathrm{e}^{2\mathrm{i}\Phi_{\mathrm{ad}}}\right] && (21)\\ &= 4S_{x,L}S_{x,R}\mathrm{e}^{-2\mathrm{i}\Phi_{\mathrm{ad}}(S_{z,L}+S_{z,R})}U_{\mathrm{CPHASE}}, && (22)\end{aligned}$$

where $U_{\mathrm{CPHASE}} = \mathrm{diag}[1,1,1,\mathrm{e}^{-2\mathrm{i}\Phi_{\mathrm{ad}}}]$. For the special case of $2\Phi_{\mathrm{ad}} = \pi$, we find for our gate

$$U_{\pi,\mathrm{ad}} = (4S_{y,L}S_{y,R})U_{\mathrm{CZ}}. \quad (23)$$

Returning to the fast pulse version of the gate, Eq. (17), we see that the same π pulses in the middle lead to

$$\begin{aligned} U_{c,\mathrm{fast}} &= U_J^{\mathrm{rf}}(t_2+T,t_2)(4S_{x,L}S_{x,R})U_J^{\mathrm{rf}}(T,0) && (24)\\ &= U_J^{\mathrm{rf}}(t_2+T,t_2)(\tau_x+\sigma_x)U_J^{\mathrm{rf}}(T,0) && (25)\\ &= (\mathbb{1}-P)\tau_x + P\mathrm{e}^{2\mathrm{i}\Phi_x}\mathrm{e}^{\mathrm{i}\delta E_z(t_2+T)\sigma_z/2}\left[c-\vec{n}\cdot\vec{\sigma}s\right] \\ &\quad\times\mathrm{e}^{-\mathrm{i}\delta E_z t_2\sigma_z/2}\sigma_x\mathrm{e}^{\mathrm{i}\delta E_z T\sigma_z/2}\left[c-\vec{n}\cdot\vec{\sigma}s\right] && (26)\end{aligned}$$

where $c = \cos(\Omega_J T)$, $s = \sin(\Omega_J T)$, $\vec{n} = (J,0,\delta E_z)/(2\Omega_J)$. In order to remove the terms proportional to $\vec{n}$ in the above, we need the action of the intermediate rotation $\mathrm{e}^{-\mathrm{i}\delta E_z t_2\sigma_z/2}\sigma_x\mathrm{e}^{\mathrm{i}\delta E_z T\sigma_z/2}$ to correspond to σ_y which requires $\sin(\delta E_z(t_2+T)/2) = \pm 1$. Furthermore, we want the equivalent unitary after the sequence,

$$\mathrm{e}^{\mathrm{i}\delta E_z/2(t_2+T)\sigma_z}\sigma_y$$

to be σ_x, which in turn requires $\delta E_z(t_2+T)/2 = (2n+1)\pi$ with integer n. Conveniently, these are the same requirement.

IV. RESONANT SINGLE STEP CNOT GATE

Additional controllability is given if the adiabatic dc exchange pulse is combined with microwave ac driving, $B_y^Q(t) \propto \cos(\omega t+\varphi)$, matching the transition frequencies between the two-qubit states which allows for direct conditional spin-flips. The gate sequence is outlined in Fig. 2 (c) and the basic concept is visualized in Fig. 2 (a) in regime III. With the exchange interaction turned on, the energy of both eigenstates $|\widetilde{\uparrow\downarrow}\rangle$ and $|\widetilde{\downarrow\uparrow}\rangle$ is lowered by $\sim J/2$, providing in total six energetically distinct resonance frequencies in the spectrum. There are four entangling transitions corresponding to the four conditional spin-flips. For example, inducing a resonant spin-flip between the states $|\uparrow\uparrow\rangle \leftrightarrow |\widetilde{\downarrow\uparrow}\rangle$ yields a CNOT with the right qubit as control and the left qubit as target gate as the following truth-table shows

$$\begin{aligned} |\uparrow\uparrow\rangle &\to |\downarrow\uparrow\rangle \\ |\uparrow\downarrow\rangle &\to |\uparrow\downarrow\rangle \\ |\downarrow\uparrow\rangle &\to |\uparrow\uparrow\rangle \\ |\downarrow\downarrow\rangle &\to |\downarrow\downarrow\rangle\,. \end{aligned} \quad (27)$$

In the remainder of this article, we always refer to this implementation of the CNOT, however, in experiments other transitions can be resonantly driven as well, giving access to a much larger set of two-qubit quantum gates.

From the eigenenergies (4)-(7) the corresponding resonance frequencies of the four conditional transitions are given as follows;

$$\begin{aligned} f^L_{|\Psi_R\rangle=|\downarrow\rangle} \equiv& |\mathcal{E}(|\downarrow\downarrow\rangle) - \mathcal{E}(|\widetilde{\uparrow\downarrow}\rangle)| \\ =& E_z + \left(-J - \sqrt{J^2+\delta E_z^2}\right)/2, && (28)\\ f^L_{|\Psi_R\rangle=|\uparrow\rangle} \equiv& |\mathcal{E}(|\widetilde{\downarrow\uparrow}\rangle) - \mathcal{E}(|\uparrow\uparrow\rangle)| \\ =& E_z + \left(J - \sqrt{J^2+\delta E_z^2}\right)/2, && (29)\\ f^R_{|\Psi_L\rangle=|\downarrow\rangle} \equiv& |\mathcal{E}(|\downarrow\downarrow\rangle) - \mathcal{E}(|\widetilde{\downarrow\uparrow}\rangle)| \\ =& E_z + \left(-J + \sqrt{J^2+\delta E_z^2}\right)/2, && (30)\\ f^R_{|\Psi_L\rangle=|\uparrow\rangle} \equiv& |\mathcal{E}(|\widetilde{\uparrow\downarrow}\rangle) - \mathcal{E}(|\uparrow\uparrow\rangle)| \\ =& E_z + \left(J + \sqrt{J^2+\delta E_z^2}\right)/2. && (31)\end{aligned}$$

One important observation is that the splitting between the conditional spin-flips is always provided by exchange,

$$f^L_{|\Psi_R\rangle=|\uparrow\rangle} - f^L_{|\Psi_R\rangle=|\downarrow\rangle} = f^R_{|\Psi_L\rangle=|\uparrow\rangle} - f^R_{|\Psi_L\rangle=|\downarrow\rangle} = J. \quad (32)$$

A. High fidelity ac implementation

We have shown so far that we can effectively cancel out a resulting CPHASE gate from the dc dynamics of our frequency selective gate by appropriately timing the length of the dc exchange pulse $t_{\mathrm{DC}} = 2\pi n/J$ where n is a positive integer. This can be thought of as applying CZ twice or any even number of times such that each CZ is cancelled out by another one due to $\mathrm{CZ}^2 = \mathbb{1}$. However, there are two additional effects which will disturb the gate if not treated appropriately. The first effect results from the off-resonant driving of nearby transitions; this effect becomes large when J is comparable to the Rabi frequency Ω of the selectively driven spin transition. A second effect originates from relative phase accumulation

of the spins during the microwave drive. Below we discuss both effects and how they can be avoided.

In the experiment described in Ref.[1] the gates are driven at the resonance frequency $\omega = f^L_{|\Psi_R\rangle=|\uparrow\rangle}$ during a dc exchange pulse which flips the left spin if and only if the right spin is in the state $|\Psi_R\rangle = |\uparrow\rangle$, thus inducing a transition between the $|\uparrow\uparrow\rangle$ and $|\widetilde{\downarrow\uparrow}\rangle$ states. However, the energy separation of the transition frequency $f^L_{|\Psi_R\rangle=|\uparrow\rangle}$ and the transition frequency for an opposite right spin, $|\Psi_R\rangle = |\downarrow\rangle$, is given by the exchange interaction strength J (see Eq. (32)). In the regime of operation [1] $\Omega \sim J \approx 20\,\mathrm{MHz}$ the transition between the states $|\uparrow\downarrow\rangle$ and $|\widetilde{\downarrow\downarrow}\rangle$ is also driven and gives rise to off-resonant Rabi dynamics. Other transitions, $f^R_{|\Psi_L\rangle=|\uparrow\rangle}$ and $f^R_{|\Psi_L\rangle=|\downarrow\rangle}$, are even further off-resonant because they are separated in energy by $\delta E_z \gg J, \Omega$, and will be neglected here.

Starting with the Hamiltonian (3) in the rotating frame $\widetilde{H}(t) = \tilde{R}^\dagger H \tilde{R} + \mathrm{i}\dot{\tilde{R}}^\dagger \tilde{R}$ with $\tilde{R} = \exp\left[-\mathrm{i}\omega t(S_{z,L} + S_{z,R})/\hbar\right]$ and neglecting fast oscillations, we find in the instantaneous adiabatic basis $\{|\uparrow\uparrow\rangle, |\widetilde{\downarrow\uparrow}\rangle, |\widetilde{\uparrow\downarrow}\rangle, |\downarrow\downarrow\rangle\}$ for $J \ll \delta E_z$

$$\widetilde{H}(t) \approx \frac{1}{2}\left(\begin{array}{cc|cc} -J + (\delta E_z + \frac{J^2}{2\delta E_z}) - \delta\omega & -\mathrm{i}\alpha_1^* & -\mathrm{i}\beta_1^* & 0 \\ \mathrm{i}\alpha_1 & -J + (\delta E_z + \frac{J^2}{2\delta E_z}) & 0 & -\mathrm{i}\beta_2^* \\ \hline \mathrm{i}\beta_1 & 0 & -J - (\delta E_z + \frac{J^2}{2\delta E_z}) & -\mathrm{i}\alpha_2^* \\ 0 & \mathrm{i}\beta_2 & \mathrm{i}\alpha_2 & J - (\delta E_z + \frac{J^2}{2\delta E_z}) + \delta\omega \end{array}\right). \quad (33)$$

Here

$$\alpha_{1,2} \approx [\pm B_y^{L,1} + B_y^{R,1} J/(2\delta E_z)]\ \mathrm{e}^{\mathrm{i}\theta}, \quad (34)$$

$$\beta_{1,2} \approx [\mp B_y^{R,1} + B_y^{L,1} J/(2\delta E_z)]\ \mathrm{e}^{\mathrm{i}\theta}, \quad (35)$$

are the effective microwave driving amplitudes after transforming into the adiabatic basis. Nearby the resonance frequency $\omega - \delta\omega = f^L_{|\Psi_R\rangle=|\uparrow\rangle} \approx E_z - \{\delta E_z + J[1 - J/(2\delta E_z)]\}/2$, $\beta_{1,2} \approx 0$, the Hamiltonian (33) decouples into two blocks, $\{|\uparrow\uparrow\rangle, |\widetilde{\downarrow\uparrow}\rangle\}$ and $\{|\widetilde{\uparrow\downarrow}\rangle, |\downarrow\downarrow\rangle\}$ which are separated in energy by $\sim \delta E_z$ (see Eq. (32)) and evolve independently in time.

For $\delta\omega = 0$, only $f^L_{|\Psi_R\rangle=|\uparrow\rangle}$ (top-left block) is resonant and yields full Rabi oscillations with a Rabi frequency $\Omega = |\alpha_1|/\hbar$ while $f^L_{|\Psi_R\rangle=|\downarrow\rangle}$ (bottom-right block) is detuned (off-resonant) by J, therefore, performing partial spin-flips with the detuned Rabi frequency $\widetilde{\Omega} = \sqrt{|\alpha_2|^2 + J^2}/\hbar$. Since the time evolution of each 2×2 block can be computed individually we find the following time evolutions of each block for the phase $\theta = 3\pi/2$ of the driving,

$$U_{|\Psi_R\rangle=|\uparrow\rangle} = \mathrm{e}^{-\frac{\mathrm{i}tf_1}{2}}\left[\cos\left(\frac{\Omega t}{2}\right)\mathbb{1} + \mathrm{i}\sin\left(\frac{\Omega t}{2}\right)\sigma_x\right], \quad (36)$$

$$U_{|\Psi_R\rangle=|\downarrow\rangle} = \mathrm{e}^{-\frac{\mathrm{i}tf_2}{2}}\left[\cos\left(\frac{\widetilde{\Omega} t}{2}\right)\mathbb{1} + \mathrm{i}\sin\left(\frac{\widetilde{\Omega} t}{2}\right) \times\left(\frac{|\alpha_2|}{2\hbar\widetilde{\Omega}}\sigma_x - \frac{J}{2\hbar\widetilde{\Omega}}\sigma_z\right)\right]. \quad (37)$$

with the frequencies $\hbar f_1 = -J + (\delta E_z + \frac{J^2}{2\delta E_z})$ and $\hbar f_2 = -\delta E_z - \frac{J^2}{2\delta E_z}$. Setting $t = \tau_{\mathrm{CNOT}} \equiv \pi(2m+1)/\Omega$ with integer m yields a spin flip in the $|\Psi_R\rangle = |\uparrow\rangle$ block. We note, that Eqs. (36) and (37) also hold for arbitrary θ under the replacement $\sigma_x \to -\cos(\theta)\sigma_x + \sin(\theta)\sigma_y$ which leads to a conditional rotation about $\boldsymbol{\mu} = (-\cos(\theta), \sin(\theta), 0)^T$ instead of CNOT (see Eq. (27) for our definition). In order to cancel the dynamics of the off-resonant states, we synchronize the Rabi frequencies by setting

$$\Omega = \frac{2m+1}{2n}\widetilde{\Omega}, \quad (38)$$

with an integer n. This can be achieved by adjusting the ac driving strength $B_y^{L,1}$. Considering $B_y^{L,1} = B_y^{R,1}$, we find the following analytical result for the ac driving strength,

$$B_y^{L,1} = a_{n,m} \equiv \pm\frac{J}{\sqrt{\frac{4n^2}{(2m+1)^2}\left(1 + \frac{J}{2\delta E_z}\right)^2 - \left(1 - \frac{J}{2\delta E_z}\right)^2}}, \quad (39)$$

with integer m and n which fulfills Eq. (38). A comparison of the dynamics with and without synchronization is depicted in Fig. 3.

At this point the time-evolution in the rotating frame $\tilde{R}$ is given by

$$U(\tau_{CNOT}) = \mathrm{e}^{-\mathrm{i}\Phi_R^{\mathrm{AC}} S_{z,R}} U_{\mathrm{CNOT}} \quad (40)$$

which is up to a local z-rotation on the right spin the desired CNOT operation. The phase Φ_R^{AC} consists of two contributions. During the CNOT gate a dynamic phase $\Phi_R^{\mathrm{AC,dyn}}$ is acquired on the right (control) spin originating from the energy difference between the two blocks in Eq. (33). While states with $|\Psi_R\rangle = |\uparrow\rangle$ are oscillating with $\mathrm{e}^{-\frac{\mathrm{i}tf_1}{2}}$, states with $|\Psi_R\rangle = |\downarrow\rangle$ oscillate with $\mathrm{e}^{-\frac{\mathrm{i}tf_2}{2}}$ which yields a relative phase after the ac spin

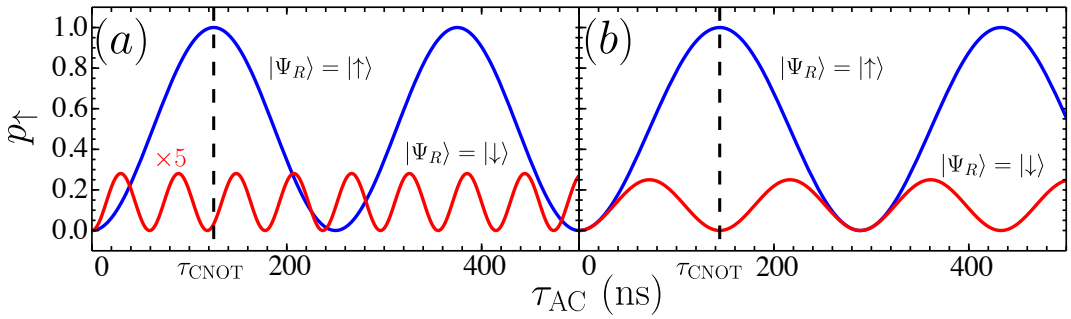

FIG. 3. Schematic plot of the resonant (blue) and off-resonant (red) transition probabilities with (a) desynchronized and (b) synchronized Rabi frequencies Ω and $\widetilde{\Omega}$ (see Eq. (38)). A CNOT gate is provided at time $\tau_{\rm CNOT}$ where the resonant driving exactly flips the spin ($p_\uparrow = 1$) for $|\Psi_R\rangle = |\uparrow\rangle$ (blue). (a) Using an arbitrary Rabi frequency Ω, we find that the frequencies are desynchronized and the off-resonant driving also yields a finite population ($p_\uparrow > 0$) of the flipped spin for $|\Psi_R\rangle = |\downarrow\rangle$ (red). (b) Synchronized resonant Rabi frequency Ω and off-resonant Rabi frequency $\widetilde{\Omega}$ which avoids any undesired population for $|\Psi_R\rangle = |\downarrow\rangle$. We choose $m = 0$ and $n = 1$ for the fastest realization of the synchronized CNOT gate yielding an ac pulse length $\tau_{\rm CNOT} \approx 144\,$ns. Note that to enhance the visibility, we rescaled the off-resonant state probabilities in (a) by a factor of 5.

flip, $\Phi_R^{\rm AC,dyn} = -(f_2 - f_1)\tau_{\rm AC}/2$, on the right spin (see Eqs. (36) and (37)). Additionally, we observe a holonomic phase[32] $\Phi_R^{\rm AC,hol}$ on the right spin which depends only on the initial and final state and does not depend on the taken path in parameter space. From Eqs. (36) and (37) it follows directly that $\Phi_R^{\rm AC,hol} = -\pi(m - n + 1/2)$ whether $\cos(\pi m) = \pm 1$ and $\sin[\pi(2m+1)/2] = \pm 1$ which only depends on the chosen time interval $\tau_{\rm CNOT}$ and the ac driving strength $B_y^{L,1}$. We find the following analytic expressions for the local S_z-rotation $\mathrm{e}^{\mathrm{i}\Phi_R S_{z,R}/2}$ on the right (control) spin after the ac spin flip,

$$\Phi_R^{\rm AC} = -\pi\left[\left(m - n + \frac{1}{2}\right) - \frac{2m+1}{a_{n,m}\left(1 + \frac{J}{2\delta E_z}\right)}\left(\delta E_z + \frac{J^2}{\delta E_z} - \frac{J}{2}\right)\right]. \tag{41}$$

The combined gate consists of the dc exchange pulse, the driven ac field, the ac phase error, Eq. (41), and the dc phase phase errors, Eqs. (11) and (12). Therefore, Eqs. (11), (12), and (41) have to be combined in order to find the total phase accumulated during the full CNOT gate. Considering the rotating frames for the dc and ac phase accumulation, we find the following results in the rotating frame of each individual spin, $R = \exp\left[-\mathrm{i}t(\omega_1 S_{z,L} + \omega_2 S_{z,R})/\hbar\right]$, with $\omega_1 = (E_z + \delta E_z/2)/\hbar$ and $\omega_2 = (E_z - \delta E_z/2)/\hbar$ (consistent with[1]);

$$\Phi_L = \Phi_L^{\rm DC} + \frac{\delta E_z}{2}\tau_{\rm DC} + \frac{\sqrt{\delta E_z^2 + J^2}}{2}\tau_{\rm AC}, \tag{42}$$

$$\Phi_R = \Phi_R^{\rm DC} - \frac{\delta E_z}{2}\tau_{\rm DC} + \Phi_R^{\rm AC} - \frac{\sqrt{\delta E_z^2 + J^2}}{2}\tau_{\rm AC}. \tag{43}$$

This additional phase can either be compensated by adjusting J such that both phases are a multiple of 2π (not possible in our regime of operation) or by including additional z-rotations on the left and right spin directly after the CNOT gate with angles $\Phi_l = 2k_1\pi - \Phi_L$ and $\Phi_r = 2k_2\pi - \Phi_R$ with integers $k_{1,2}$. Simulations where we numerically integrate the time-dependent Schrödinger equation $i\hbar\dot{\Psi}(t) = \widetilde{H}(t)\Psi(t)$ for the full Hamiltonian (33) support our analysis (see Fig. 4). The highest fidelity can indeed be found after correcting the described phase shifts. At this point it is worth mentioning that z-rotations in the experiment in Ref.[1] and similar experiments [9,10] can be performed by modifying the reference phase for the individual spins. This can be done rapidly and accurately in software with no additional microwave control required.

B. Charge noise analysis

In semiconductor devices charge noise is omnipresent[33]. In the simplest model, charge noise can be described as fluctuations of the electric potentials near the dot. Thus, charge noise couples to the two-qubit systems mainly through the exchange interactions due to its dependence on the detuning, tunneling, and confinement of the spins[16,17]. To be precise, charge noise couples also to single spins through the same mechanism that allows EDSR to rotate the spin though fluctuations of the electron positions. This effect, however, is small as evidenced by Ref.[10], thus will be neglect in the analysis below.

In lowest order $J \to J + \delta J$ where δJ are fluctuations of the exchange energy due to charge noise, we find the following first-order corrections to the diagonal Hamilto-

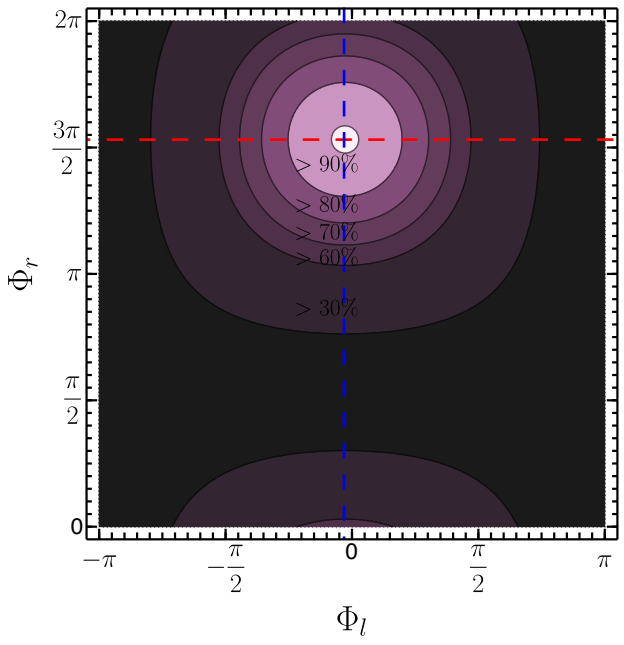

FIG. 4. Simulated CNOT gate fidelity (in percent) as a function of the compensated phase Φ_L and Φ_R on the left spin (target) and right spin (control) after the ac drive. Compensation is provided for a z-rotation $\hat{Z}(\Phi)$ on the left spin with $\Phi_l = 2\pi k_l - \Phi_L$ and on the right spin $\Phi_r = 2\pi k_r - \Phi_R$ with integers k_l and k_r, thus $\Phi = (\Phi_l, \Phi_r) \approx (-0.03\pi, -0.469\pi)$ (blue and red dashed lines). For the simulation we used the following parameters related to the experiment in Ref.[1]; $J = 19.7\,\mathrm{MHz}$, $\delta E_z = 210\,\mathrm{MHz}$, $\tau_r = 5\,\mathrm{ns}$, $\tau_{\mathrm{CNOT}} = 94\,\mathrm{ns}$ (corresponding to $\alpha = 1/(2\tau_{\mathrm{CNOT}})$, $\tau_{\mathrm{DC}} = 198\,\mathrm{ns}$, and $m = 0$ and $n = 1$ in Eq. 38)

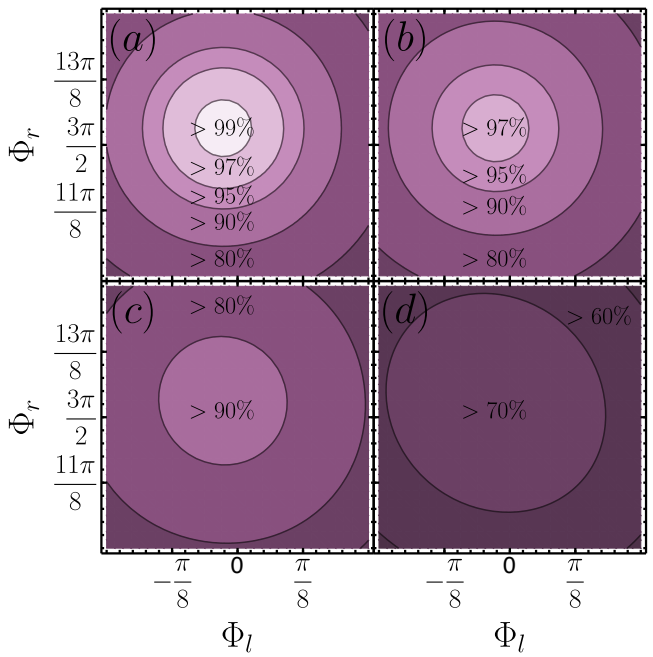

FIG. 5. Zoom in of the simulation in Fig. 4 in the presence of charge noise fluctuations with strength (a) $\sigma_{\delta J} = 0\,\mathrm{MHz}$, (b) $\sigma_{\delta J} = 0.33\,\mathrm{MHz}$, (c) $\sigma_{\delta J} = 0.67\,\mathrm{MHz}$, and (d) $\sigma_{\delta J} = 1.33\,\mathrm{MHz}$. For the simulation the fluctuations are assumed to be quasistatic and Gaussian distributed with standard deviation $\sigma_{\delta J}$ and mean $\langle \delta J \rangle \approx 0$.

nian (4)-(7) in the adiabatic basis $\{|\uparrow\uparrow\rangle, |\widetilde{\downarrow\uparrow}\rangle, |\widetilde{\uparrow\downarrow}\rangle, |\downarrow\downarrow\rangle\}$

$$H_{\mathrm{noise}} = \frac{2J\delta J}{\delta E_z}(\widetilde{S}_z^L + \widetilde{S}_z^R) - 2\delta J \widetilde{S}_z^L \widetilde{S}_z^R. \qquad (44)$$

The first term in Eq. (44) induces single-qubit dephasing but is highly suppressed in the case where $J \ll \delta E_z$ since it has strength $\propto J/\delta E_z$. Therefore, large magnetic field gradients are beneficial for operating the two-qubit gate. The second term couples longitudinally to the two-qubit gate operation since it has the same form as the dc pulse, $\propto S_z^L S_z^R$, and reduces the fidelity of the resulting two-qubit gate that only depends on the bare charge noise fluctuations δJ. In experiments[9], this is the limiting factor for the gate fidelity, since simple echo protocols would also filter out the desired two-qubit interaction ruling out their use. Simulations assuming quasistatic noise show that for $\sigma_{\delta J} \equiv \sqrt{\langle \delta J^2 \rangle - \langle \delta J \rangle^2} = 0.33\,\mathrm{MHz}$ two-qubit gate fidelities $> 97\%$ are still possible (see Fig. 5 (b)). However, fluctuations twice (four times) as large already limit the gate fidelity to about $\approx 93\%$ ($\approx 77\%$) (see Fig. 5 (c) and (d)), which is problematic for fault-tolerant quantum computation. However, mitigation of these effects is still possible through advanced pulse shaping[34], composite pulse sequences[35], complex dynamical decoupling sequences[36], and a reduction of the amplitude of the fluctuations, i.e., operating at a charge noise sweet spot.

V. CONCLUSION

In this paper, we have presented high-fidelity implementations of a dc-pulsed CZ gate and a single-shot resonant CNOT gate.

For the dc-pulsed CZ gate, we have provided a high-fidelity implementation using dc exchange pulses. We have analyzed two regimes for the exchange pulses, slow (adiabatic) and fast (instantaneous) exchange pulses, and have described how to compensate for residual spin-flip and phase errors. In the adiabatic regime, spin-flip errors are suppressed by the magnetic field difference and we have identified the phases that the individual spins accumulate during the two-qubit operation. By interrupting the CZ gate with single-qubit spin-flips to form a spin-echo sequence, spin-flip errors and local phases which the individual spins acquired during the CZ gate can be avoided even for the non-adiabatic exchange pulses.

For the single-shot resonant CNOT gate, we have presented a high-fidelity implementation through frequency-

selective resonant modulations of the two-qubit transitions. By selecting different transition frequencies a larger set of two-qubit quantum gates is accessible allowing for more efficient algorithms. We have shown that all intrinsic errors due to all relevant off-resonant transitions can be compensated by fine-tuning the ac driving amplitude such that the resonant and the off-resonant oscillations are synchronized. Additionally, we have identified phases which the individual spins accumulate during the two-qubit operation. These phases can be compensated for by performing single-qubit z-rotations after each CNOT gate. Our two-qubit gate implementation also incorporates a reduction of charge noise by suppression through large magnetic field gradients and a partial intrinsic spin-echo decoupling sequence. Using the synchronization technique and the analytic values of the accumulated phases, we predict that existing experiments will be able to reach higher two-qubit gate fidelities exceeding 97% under realistic assumptions. This opens the path to large-scale quantum computation previously limited by low-fidelity two-qubit gates.

ACKNOWLEDGMENTS

Research was sponsored by Army Research Office grant W911NF-15-1-0149, the Gordon and Betty Moore Foundation's EPiQS Initiative through grant GBMF4535, and NSF grant DMR-1409556. This research was partially supported by NSF through the Princeton Center for Complex Materials, a Materials Research Science and Engineering Center DMR-1420541.

[1] D. M. Zajac, A. J. Sigillito, M. Russ, F. Borjans, J. M. Taylor, G. Burkard, and J. R. Petta, Science (2017), 10.1126/science.aao5965.
[2] D. Loss and D. P. DiVincenzo, Phys. Rev. A **57**, 120 (1998).
[3] F. A. Zwanenburg, A. S. Dzurak, A. Morello, M. Y. Simmons, L. C. L. Hollenberg, G. Klimeck, S. Rogge, S. N. Coppersmith, and M. A. Eriksson, Rev. Mod. Phys. **85**, 961 (2013).
[4] M. Steger, K. Saeedi, M. L. W. Thewalt, J. J. L. Morton, H. Riemann, N. V. Abrosimov, P. Becker, and H. J. Pohl, Science **336**, 1280 (2012).
[5] A. M. Tyryshkin, S. Tojo, J. J. L. Morton, H. Riemann, N. V. Abrosimov, P. Becker, H.-J. Pohl, T. Schenkel, M. L. W. Thewalt, K. M. Itoh, and S. A. Lyon, Nat Mater **11**, 143 (2012).
[6] M. Veldhorst, J. C. C. Hwang, C. H. Yang, A. W. Leenstra, B. de Ronde, J. P. Dehollain, J. T. Muhonen, F. E. Hudson, K. M. Itoh, A. Morello, and A. S. Dzurak, Nat Nano **9**, 981 (2014).
[7] M. Veldhorst, C. H. Yang, J. C. C. Hwang, W. Huang, J. P. Dehollain, J. T. Muhonen, S. Simmons, A. Laucht, F. E. Hudson, K. M. Itoh, A. Morello, and A. S. Dzurak, Nature **526**, 410 (2015).
[8] K. Takeda, J. Kamioka, T. Otsuka, J. Yoneda, T. Nakajima, M. R. Delbecq, S. Amaha, G. Allison, T. Kodera, S. Oda, and S. Tarucha, Sci Adv **2**, e1600694 (2016).
[9] T. F. Watson, S. G. J. Philips, E. Kawakami, D. R. Ward, P. Scarlino, M. Veldhorst, D. E. Savage, M. G. Lagally, M. Friesen, S. N. Coppersmith, M. A. Eriksson, and L. M. K. Vandersypen, arXiv:1708.04214.
[10] J. Yoneda, K. Takeda, T. Otsuka, T. Nakajima, M. R. Delbecq, G. Allison, T. Honda, T. Kodera, S. Oda, Y. Hoshi, N. Usami, K. M. Itoh, and S. Tarucha, Nat Nano (2017), 10.1038/s41565-017-0014-x.
[11] D. Lidar and T. Brun, *Quantum Error Correction* (Cambridge University Press, 2013).
[12] R. Brunner, Y.-S. Shin, T. Obata, M. Pioro-Ladrière, T. Kubo, K. Yoshida, T. Taniyama, Y. Tokura, and S. Tarucha, Phys. Rev. Lett. **107**, 146801 (2011).
[13] D. M. Zajac, T. M. Hazard, X. Mi, E. Nielsen, and J. R. Petta, Phys. Rev. Applied **6**, 054013 (2016).
[14] M. Pioro-Ladriere, T. Obata, Y. Tokura, Y. S. Shin, T. Kubo, K. Yoshida, T. Taniyama, and S. Tarucha, Nat Phys **4**, 776 (2008).
[15] T. Otsuka, T. Nakajima, M. R. Delbecq, S. Amaha, J. Yoneda, K. Takeda, G. Allison, T. Ito, R. Sugawara, A. Noiri, A. Ludwig, A. D. Wieck, and S. Tarucha, Scientific Reports **6**, 31820 (2016).
[16] G. Burkard, D. Loss, and D. P. DiVincenzo, Phys. Rev. B **59**, 2070 (1999).
[17] S. Das Sarma, X. Wang, and S. Yang, Phys. Rev. B **83**, 235314 (2011).
[18] J. R. Petta, A. C. Johnson, J. M. Taylor, E. A. Laird, A. Yacoby, M. D. Lukin, C. M. Marcus, M. P. Hanson, and A. C. Gossard, Science **309**, 2180 (2005).
[19] B. Bertrand, H. Flentje, S. Takada, M. Yamamoto, S. Tarucha, A. Ludwig, A. D. Wieck, C. Bäuerle, and T. Meunier, Phys. Rev. Lett. **115**, 096801 (2015).
[20] F. Martins, F. K. Malinowski, P. D. Nissen, E. Barnes, S. Fallahi, G. C. Gardner, M. J. Manfra, C. M. Marcus, and F. Kuemmeth, Phys. Rev. Lett. **116**, 116801 (2016).
[21] M. D. Reed, B. M. Maune, R. W. Andrews, M. G. Borselli, K. Eng, M. P. Jura, A. A. Kiselev, T. D. Ladd, S. T. Merkel, I. Milosavljevic, E. J. Pritchett, M. T. Rakher, R. S. Ross, A. E. Schmitz, A. Smith, J. A. Wright, M. F. Gyure, and A. T. Hunter, Phys. Rev. Lett. **116**, 110402 (2016).
[22] C. Zhang, R. E. Throckmorton, X.-C. Yang, X. Wang, E. Barnes, and S. Das Sarma, Phys. Rev. Lett. **118**, 216802 (2017).
[23] X.-C. Yang and X. Wang, Phys. Rev. A **96**, 012318 (2017).
[24] J. M. Nichol, L. A. Orona, S. P. Harvey, S. Fallahi, G. C. Gardner, M. J. Manfra, and A. Yacoby, npj Quantum Information **3**, 3 (2017).
[25] G. Burkard, D. Loss, D. P. DiVincenzo, and J. A. Smolin, Phys. Rev. B **60**, 11404 (1999).
[26] T. Meunier, V. E. Calado, and L. M. K. Vandersypen, Phys. Rev. B **83**, 121403 (2011).
[27] S. E. Economou and E. Barnes, Phys. Rev. B **91**, 161405 (2015).
[28] H. S. Ku, J. L. Long, X. Wu, M. Bal, R. E. Lake, E. Barnes, S. E. Economou, and D. P. Pappas, Phys. Rev. A **96**, 042339 (2017).

[29] J. Levy, Phys. Rev. Lett. **89**, 147902 (2002).
[30] W. M. Witzel, I. Montano, R. P. Muller, and M. S. Carroll, Phys. Rev. B **92**, 081407 (2015).
[31] C. Jones, M. F. Gyure, T. D. Ladd, M. A. Fogarty, A. Morello, and A. S. Dzurak, arXiv:1608.06335.
[32] E. Sjöqvist, Physics Letters A **380**, 65 (2016).
[33] E. Paladino, Y. M. Galperin, G. Falci, and B. L. Altshuler, Rev. Mod. Phys. **86**, 361 (2014).
[34] E. Barnes, X. Wang, and S. Das Sarma, Scientific Reports **5**, 12685 (2015).
[35] L. M. K. Vandersypen and I. L. Chuang, Rev. Mod. Phys. **76**, 1037 (2005).
[36] A. De and L. P. Pryadko, Phys. Rev. A **89**, 032332 (2014).